
Article:
Wilkes, M., Mukherjee, S. and Brown, S. orcid.org/0000-0001-8229-8004 (2021) Transient CO2 capture for open-cycle gas turbines in future energy systems. Energy, 216. 119258. ISSN 0360-5442

https://doi.org/10.1016/j.energy.2020.119258

Transient CO_2 capture for open-cycle gas turbines in future energy systems

Mathew Dennis Wilkes[a], Sanjay Mukherjee[a] Solomon Brown[a]*.

[a] Department of Chemical and Biological Engineering, University of Sheffield, Sheffield, S1 3JD, United Kingdom
*** Corresponding Author:** Solomon Brown
Email: s.f.brown@sheffield.ac.uk
Telephone: +44 (0) 114 2227597

Abstract:

In complex electricity systems with a varied generation mix, the security of supply is important, and the quick-response nature of gas turbines is invaluable in providing system flexibility. Accompanied with post-combustion capture (PCC) of CO_2, gas turbines can support the transition to a future low-carbon electricity system.

This study presents the development and validation of a dynamic rate-based model of the benchmark CO_2 absorption process, using 30 wt.% monoethanolamine (MEA). The model is scaled up from pilot-scale to match the flue gas output from a modern small-scale gas turbine operating in open-cycle configuration. Simulations of various flexible operating scenarios shows the rapid transitioning between full and partial load is beneficial in delivering higher time-averaged CO_2 capture rates, compared to the Baseload scenario where the PCC system is operated at full load for five hours. Maintaining a constant liquid/gas (L/G) ratio results in 90.01% CO_2 capture; however, this increases the energy demand due to constant reboiler steam flowrate. To compensate, the steam flowrate is also ramped, resulting in a small decrease in reboiler duty compared to the Baseload scenario. Importantly, no negative energy or capture rate related issues to highly-transient PCC operation are found.

Key Words:

CO_2 capture, Dynamic Modelling, Post-combustion capture, Flexible Operation, Gas Turbine

1. Introduction

Energy systems globally are transitioning away from conventional fossil fuels. It is well known that the transition from a carbon-intense energy system requires balancing capacity, due to the realistic constraints created by a high penetration of intermittent renewables (see for example Heuberger and Mac Dowell [1]). One such constraint is the need for increased system flexibility. The flexibility of an energy system is its ability to respond to fluctuations in generation and demand [2]. In the UK, the National Grid has various reserve and balancing services used to correct generation imbalances and demand-side response [3]. Electricity systems also rely on connected synchronous generators to provide grid inertia to minimise the frequency disturbances created by an imbalance between generation and demand [4]. In the future low-carbon electricity system, the fast ramping rates and operating flexibility of gas turbines, can play a vital role in providing both grid inertia and acting as a balancing service [5]. However, to continue on the path to developing a low-carbon energy system, these quick-response generators will require Carbon Capture, Utilisation and Storage (CCUS), a key research requirement identified in Brown et al. [6].

A modern gas turbine (GT) typically has a gross electrical efficiency between 30-40% and coupled with low-NO_X burners produce less than 25 ppm of NO_X at 15% O_2. Table 1 shows currently available GTs, with an electrical power output less than 50 MW. The figures presented are for open/simple cycle configuration. Open-cycle gas turbine (OCGT) power stations have no heat recovery steam generation (HRSG), as a result they have quick start-up and shutdown times. The average ramp rate is between 8-12% of maximum load per minute, and the hot and cold start-up times are 5-11 minutes [7].

Table 1: Current small-scale gas turbines on the market

Gas Turbine	MHPS H-25 Series	GE TM2500	SIEMENS SGT-600	Caterpillar TITAN™ 130	SIEMENS SGT-400
Power Output (MWe)	41.0	33.7	24.5	16.5	10.4
Exhaust Flowrate (kg/s)	114.0	-	81.3	55.8	33.8
Exhaust Temperature (°C)	569.0	-	543.0	485.0	508.0
NOx Level (ppm)	15.0	25.0	≤9	-	≤25.0
Efficiency (%)	36.2	35.0	33.6	35.5	34.8
Sources	[8]	[9]	[10]	[11]	[10]

To prevent altering combustion dynamics this study focuses on post-combustion capture (PCC) of CO_2. The benchmark PCC technology is solvent-based chemical absorption using 30 wt.% monoethanolamine (MEA) with 90% CO_2 capture rate, leading to a typical reboiler duty between 3.6-4.0 GJ/tonne CO_2 [12]. The reboiler duty can be decreased through process intensification [13, 14, 15, 16], however, this study focuses on the conventional process configuration with no modifications or optimisation.

To transition to a low-carbon future and maintain security of electricity supply, understanding the dynamic behaviour of PCC on flexible fossil power is of the utmost importance [17]. The necessity and role CCUS can play in future energy system is explained by Domenichini et al. [18], Heuberger et al. [19] and Mac Dowell and Staffell [20]. It can even be economically beneficial by exploiting higher electricity prices during peak periods [21]. Several simulation based studies have investigated operational flexibility of coal- and gas-PCC, focussing on comparing operating strategies [22, 23, 24], developing process control strategies [25, 26], and multi-period optimisation [27]. Montañés et al. [28] identifies the operational requirements of flexible CO2 capture, and concluded future work should consist of validated dynamic process models evaluating various transient operating scenarios, to discover potential bottlenecks during flexible operation. More information on pilot-scale dynamic PCC operation can be found in Section 3.

The majority of the flexible PCC literature revolves around large-scale power sources >300MW and some work has been done on micro-gas turbines <1MW [29]. To the authors knowledge no studies have focused on the transient operation of absorption-based PCC on small-scale fossil power sources (>1MW to <50MW). This study aims to fill this gap in the literature and focuses on PCC for OCGT power plants, due to their expected growth in the UK energy market [1]. Since, these power sources have no HRSG units, there is no possibility of re-routing reboiler steam for increased power output in a frequency response scenario [30].

With the role small-scale decentralised power can play in decarbonising the energy sector, this study analyses the transient behaviour of OCGTs in the UK electricity system. This data is translated into exhaust gas flowrates and used to simulate the flexible operation of a small–scaled CO_2 absorption facility using MEA as the solvent. The transient nature of (OCGT) power plants is assessed using data from the Balancing Mechanism Reporting Service (BMRS) and industrial suppliers. This study addresses the possible complexities of PCC integrated OCGT systems through:

- evaluating transient operational behaviour of OCGT power generation
- development and validation of a dynamic model for an amine-based PCC process
- assessing the flexible response of PCC under different operating scenarios

The remainder of this paper is structured as follows: gas turbine operation, flexible PCC operation, description of the capture model, dynamic model validation against dynamic pilot-scale data, and results for the scaled PCC plant attached to a 10 MWe OCGT power plant.

2. Gas Turbine Operation

To evaluate the transient operation of an OCGT plant, data is analysed from the BMRS, which provides operational data on the balancing and settlement arrangements in Great Britain (GB), with a 30 minute time interval [31]. Figure 1 is a compilation of OCGT generation over the last four years in the GB. The data is grouped per generation type, individual loads each power station are not reported. OCGT plants come on the system as a balancing service during periods of high demand, typically used in the colder months of January, February and December. The maximum load on the system for that given year is dependent on the amount of generation contracted in the capacity auction market and therefore changes each year.

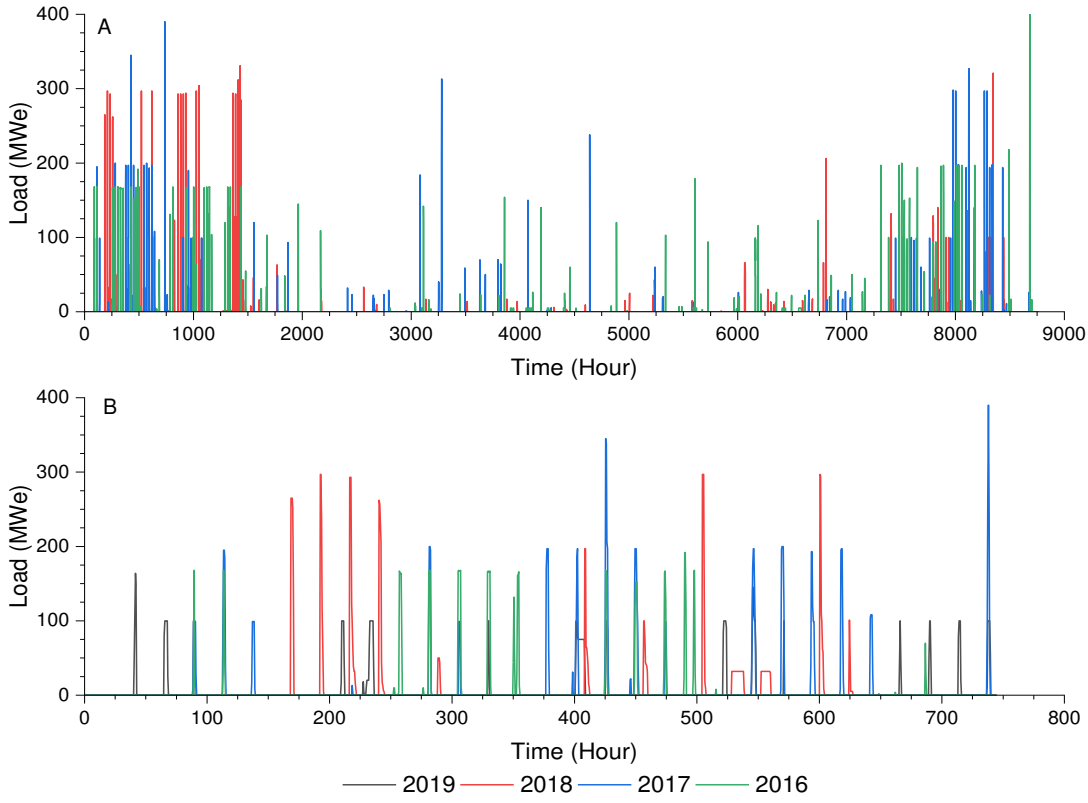

Figure 1: Half hourly OCGT generation over previous four years in Great Britain (GB), showing data for A) the entire year and B) January

Figure 2 compares the time of day OCGT generation has come on in the month of January over the last 4 years. Over this 744-hour period, OCGT generation comes on the system on average of 15 times but ranges between 12 to 17 times. Typically, active between 15:00-20:00, corresponding the peak daily demand in GB. In 2018, OCGT generation was on the system mostly overnight instead of in the evenings, as a result of severe weather conditions. However, the plants still operated for a similar amount of time averaging 5 hours per day. The maximum annual operation over the previous four years was in 2018 with 230 hours. The difficulty lies with predicting these ramping cycles, in order to develop suitable control strategies for efficient PCC performance. For instance, several days show two distinct peaks with several hour gaps in between. Also, OCGTs typically have one major power output peak per operating cycle (from start-up to shutdown), however, the magnitude and time-scale of these peaks vary. Combining this with the information in Figure 1, shows multiple periods

where the power output has changed, and the new power output is maintained for several hours. The key observations from the BMRS data for OCGT generation are as follows:

- sporadic operation largely deployed in the winter months
- used for peak demand typically in the evenings
- highly transient behaviour i.e. ramping to different power outputs during the same operating cycle, with multiple operating cycles within a 24-hour period
- average operating cycle is 5 hours
- total power generated from OCGT's varies annually

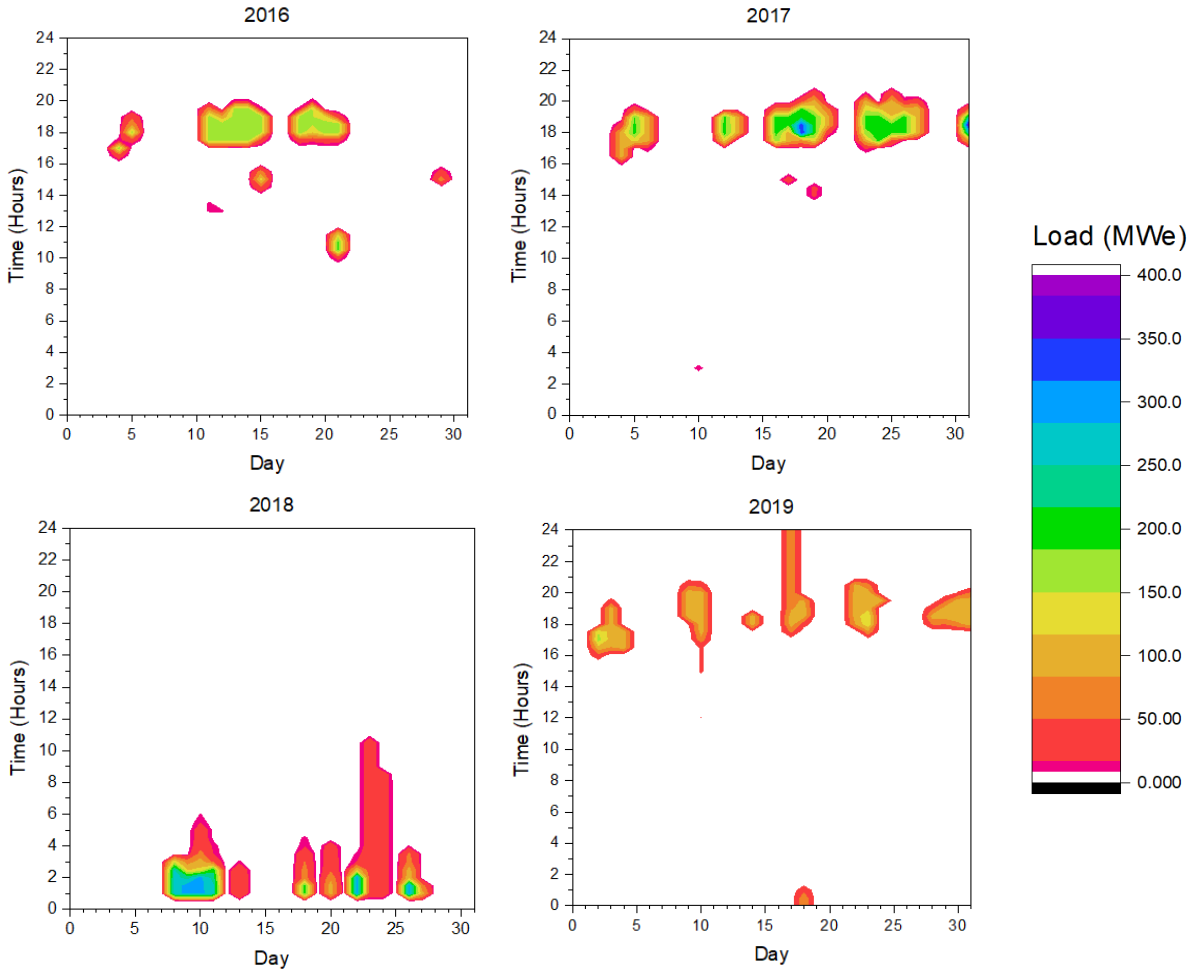

Figure 2: Contour plot of OCGT generation in January over the previous four years in the GB

3. Dynamic PCC Operation

Operating a capture plant with a high degree of transient operation can affect the performance of the process, and several studies shown in Table 2 have presented experimental results for dynamic PCC operation.

Tait et al. [30] performed a set of dynamic experiments on gas-PCC, using 30 wt. % MEA at the Sulzer Chemtech pilot-scale facility in Winterthur, Switzerland. The authors presented five different dynamic operating scenarios, including a frequency response scenario where the steam flowrate to the reboiler increases by 200%, representative of a situation where power output needs to be rapidly decreased to maintain grid frequency within allowable limits. The study highlighted no significant barriers to flexible use of gas PCC and suggests altering power output every 30 minutes to match settlement period in GB.

Table 2: Pilot plants evaluating flexible operation and performance of PCC using MEA as the solvent

Pilot Facility	Flue Gas Source	Flue Gas Flowrate	Source
Brindisi, Italy	Coal	10,000 Nm^3/h [a]	[32]
CSIRO, Australia	Brown-Coal	50 kg/h	[33]
Sulzer Chemtech, Switzerland	Natural Gas	120.5 Nm^3/h [a]	[30]
Technology Centre Mongstad, Norway	Natural Gas	60,000 Sm^3/h [b]	[34]
PACT, England	Coal	200 Nm^3/h [a]	[35]

[a] N stands for nominal, which is at 0°C and 1 atm, [b] S stands for standard, which is 15°C and 1 atm

Montañés et al. [34] presented experimental results for the transient performance of control mechanisms for flexible PCC operation, for treatment of flue gas from a combined cycle combined heat and power plant at Technology Centre Mongstad (TCM). The dynamic experiments changed the flue gas, solvent, and steam flowrates to investigate capture plant ramping. These are also the main three parameters manipulated in Tait et al. [35]. The capture plant ramping scenario is similar to the benchmark flexible operating scenario in Mac Dowell and Shah [36]. The results in Montañés et al. [34] showed that following a perturbation, the system took approximately 1 hour to reach steady-state. Bui et al. [37] reported three flexible operating scenarios at the TCM capture facility, accompanied with dynamic modelling. The study found the stabilisation time (to allow complete solvent circulation and homogenous solvent compositions) is a minimum of three hours. Also, the demonstration scale plant took as long as 114 minutes to transition to new operating conditions following a change in one or more of the main process parameters. This is known as the transition time, and is difficult to incorporate into process models, and Bui et al. [37] concludes further improvements in the dynamic response of PCC models is required.

Here, to analyse the flexible PCC operation, we study the changes during dynamic operating scenarios and the effect of these on the capture process. From Table 1, the relationship between the power output and the exhaust gas flowrate is linear, therefore, any changes in power directly corresponds to exhaust flowrates. Bellas et al. [38] showed the changes in gas turbine exhaust composition during different power outputs, however, incorporating this aspect is beyond the scope of this study. In future energy systems, the behaviour of OCGT generation may not be identical to that shown in Section 2, so here we focus on one of the most challenging scenarios exhibited in a real system. To this end, we simulate PCC operation during start-up, ramping to 70% and 50% full load, and shutdown. Each operating scenario utilises a load following strategy, where flue gas, solvent and steam flowrate changes are directly proportional to the power output. The operating scenarios:

- **Baseload:** This scenario includes the start-up and shutdown for the flue gas, solvent and reboiler steam streams, there is no ramping of the flue gas as the GT in this scenario is at full load for the entire five-hour operation.
- **Scenario A:** Only changing the flue gas flowrate, i.e. the capture plant parameters remain constant during full load operation. For comparative reasons, the start-up and shutdown procedures are also included.
- **Scenario B:** Maintaining a constant L/G ratio, throughout the literature this is as common load following technique [25]. Changing the lean solvent flowrate proportional

to the flue gas flowrate encourages a constant capture rate, in reality the capture rate increases due to higher absorber residence times [22].

- **Scenario C:** Maintaining a constant L/G ratio and reducing steam flowrate to the reboiler. In order to maintain constant conditions during transient operation the flowrate of steam to the reboiler is decreased.

This study uses the Siemens SGT-400 as an example modern gas turbine, shown in Table 1, the 11 MW version produces 33.8 kg/s of exhaust mass flow with low NO_X (≤25 ppm). The rated power output in open-cycle configuration is 10.4 MWe [10]. Assuming the exhaust temperature can be brought down to a suitable inlet absorber temperature through a heat recovery unit, the waste heat can be used to generate the steam necessary for solvent generation. The dynamic model is scaled up to handle 33.8 kg/s of exhaust gas. Based on average data from [7] the start-up and shutdown rates are 12.5% baseload per minute, and the ramping rates are 10% baseload per minute. Figure 3 shows the flowrate changes throughout each operating scenario as a percentage of the baseload operation. Each new power output is maintained for 1 hour, or two settlement periods based of the balancing and settlement period in GB. The aim of the case study is to compare the flexible operating scenarios against the Baseload case, to highlight the effects of ramping various process parameters. The scaled capture plant consists of non-optimised equipment sizes and is used for comparative analysis not process design.

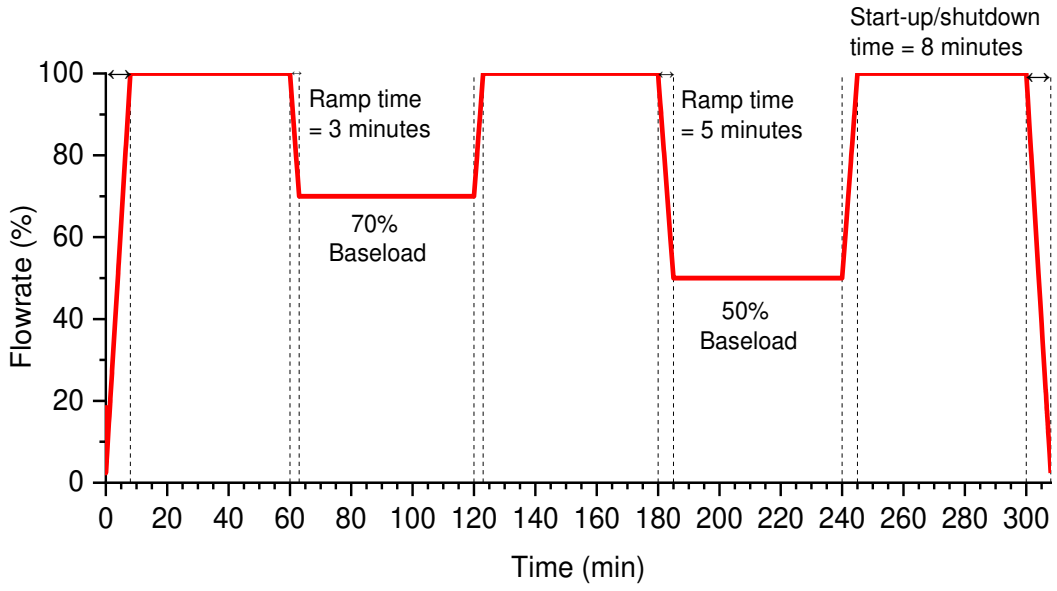

Figure 3: Flue gas, solvent and reboiler steam flowrate changes throughout the operating scenarios

4. Capture Plant Model Description

The complex reaction chemistry and process design of amine-absorption can be captured through steady-state modelling. However, to capture the transient process behaviour, high-fidelity dynamic models must be used to account for any variation due to time. Chikukwa et al. [39], Bui et al. [40] and Wu et al. [41] have reviewed dynamic modelling of amine-absorption, and showed through-out the literature simulations using a rate-based approach yield more accurate predictions of key process parameters. For rate-based simulations the multi-component mass and heat transfer in a packed absorption/desorption column is described by two-film theory, where an infinitesimally thin interface separates the liquid and gas films. For this study each column is represented by a cascade of non-equilibrium

stages (j). Assuming negligible radial variation of properties and minimal solvent degradation, the material balances for component i in the liquid and gas phases are [42]:

$$\frac{\partial M_{i,j}^{L}}{\partial t} = \frac{\partial L_{i,j}}{\partial z} + \mathcal{N}_{\mathrm{i,j}}^{L} \quad i = 1, \dots, c, \;\; j = 1, \dots, \mathrm{n} \tag{1}$$

$$\frac{\partial M_{i,j}^{G}}{\partial t} = \frac{\partial G_{i,j}}{\partial z} - \mathcal{N}_{\mathrm{i,j}}^{G} \quad i = 1, \dots, c, \;\; j = 1, \dots, \mathrm{n} \tag{2}$$

Where M is the molar holdup or accumulation of components i to c in stages j to n, axially distributed across height z (m), L is the liquid molar flow (kmol/s) and V is the vapour molar flow (kmol/s). The superscripts L and G denote the liquid and gas phases, respectively. At any position in the column there must be continuity between the molar fluxes ($\mathcal{N}$) across the interface, which are functions of the mass transfer coefficients for the gas and liquid flows [43]. Mores et al. [44] compared mass transfer correlations for MEA-CO_2 desorption from Bravo and Fair [45] and Onda et al. [46] using experimental data from Dugas [47]. The report concluded the correlation in Onda et al. [46] was more suitable due to the overall smaller deviation between predicted and experimental values. Onda et al. [46] developed the following mass transfer correlations for gas absorption and desorption systems:

$$k_{i,j}^{L} = 0.0051 \left(\frac{L}{a_w \mu_L}\right)^{\frac{2}{3}} \left(\frac{\mu_L}{\rho_L D_L}\right)^{-\frac{1}{2}} \left(a_t d_p\right)^{0.4} \left(\frac{\mu_L g}{\rho_L}\right)^{0.333} \tag{3}$$

$$k_{i,\mathrm{j}}^{G} = 5.23 \left(\frac{G}{a_t \mu_G}\right)^{0.7} \left(\frac{\mu_G}{\rho_G D_G}\right)^{\frac{1}{3}} \left(a_p d_p\right)^{-2} \left(\frac{\mathrm{RT}}{\mathrm{a_T d_p}}\right)^{-1} \tag{4}$$

Where k is the mass transfer co-efficient of component i in the liquid (m/s) and gas phases (kg.mol/m^2.s.atm), a_T is the total packing surface area (m^2/m^3), a_w is the wetted packing surface area (m^2/m^3), μ is the viscosity (kg/m.s), d_p is the packing nominal size (m), g is the acceleration due to gravity (m/s^2), ρ is density (kg/m^3), D is the diffusion coefficient (m^2/s), R is the gas constant (m^3.atm/kg.mol.K) and T is the temperature (K). Phase equilibrium is assumed at the vapour-liquid interface, and chemical equilibrium is assumed in the entire liquid phase. Reactions are treated implicitly and the thermophysical properties are described through the Statistical Associating Fluid Theory (SAFT) properties package gSAFT-VR [48]. The fluid phase behaviour of CO_2 in aqueous MEA described by gSAFT-VR is discussed at length in Mac Dowell et al. [49]. The pressure drop over each spatial element is modelled using the approach in Billet and Schultes [50] for irrigated random or structured packing, the overall equation is:

$$\frac{\partial P}{\partial z} = \psi_L \frac{a_W}{(\varepsilon - h_l)^3} \frac{F_G^2}{2} \frac{1}{K} \tag{5}$$

Where P is pressure (Pa), ψ_L is the resistasnce coefficient, ε is the void fraction, h_l is the liquid holdup, F_G is the gas capacity factor ($Pa^{0.5}$), and K is the wall factor. A more detailed explanation of the equations and limits is shown in Billet and Schultes [50]. Under adiabatic conditions, the energy balances for the liquid and gas phases are [51]:

$$\frac{\partial U_j^{L}}{\partial t} = \frac{\partial H_j^{L}}{\partial z} + \varepsilon_j^{L} \quad j = 1, \dots, n \tag{6}$$

$$\frac{\partial U_j^{V}}{\partial t} = \frac{\partial H_j^{V}}{\partial z} - \varepsilon_j^{V} \quad j = 1, \dots, n \tag{7}$$

Where U is the energy holdup or accumulation of energy in that phase on stage j to n. H is the energy flow (kJ/s), and $\boldsymbol{\varepsilon}$ is the energy flux across the interface (kJ/s). Figure 4 shows the model topology of a conventional amine-absorption process, developed in gPROMS® gCCS 1.1.0. The model includes the dynamic operation of the condenser, reboiler, and heat-exchanger units. For non-equilibrium stage models for multicomponent distillation, the reboiler and condenser units can be considered equilibrium stages, and are modelled using the MESH equations described in Taylor and Krishna [43]. The heat exchangers are modelled using the number of transfer units (NTU) method, described in Shah and Sekulić [52]. The heat transfer area is calculated to give the desired rich-solvent temperature prior to entering the stripping column. This assumes the system is under adiabatic conditions, with a fixed heat transfer coefficient and pressure drop [48]. The height of packing for the absorber and stripping columns are scaled using the transfer unit method described in Mores et al. [44].

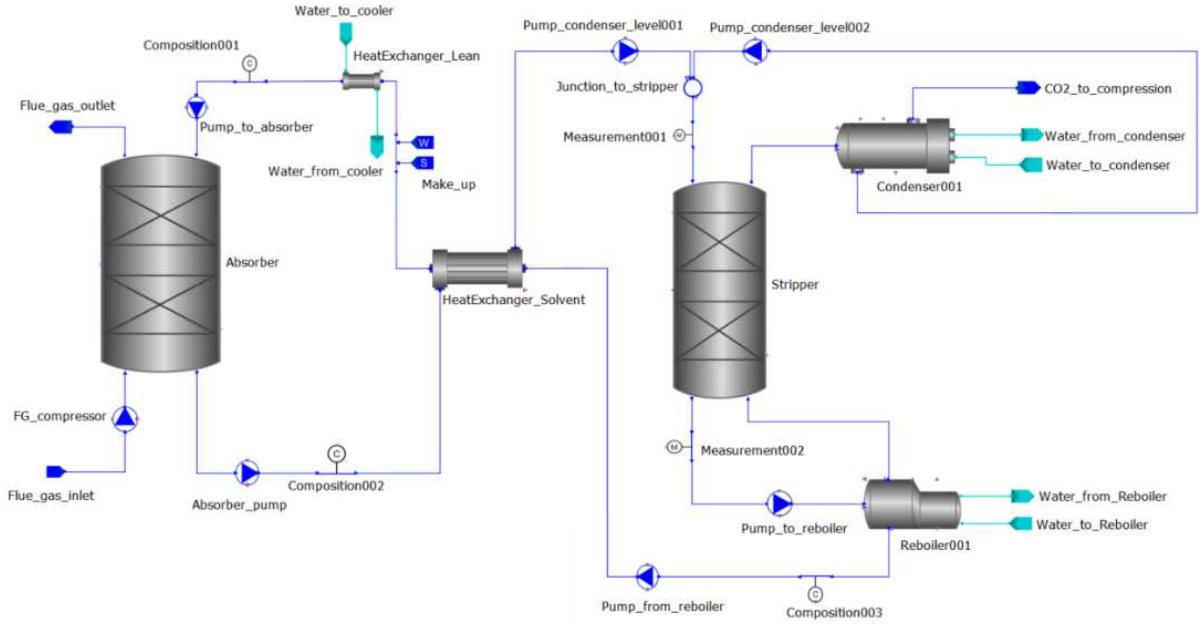

Figure 4: Model topology of a conventional amine-absorption process

Throughout the literature, CO_2 capture technologies are analysed and compared through capture efficiency and energy demand. In this study, the key operating parameter is the CO_2 capture rate and a key process indicator is the reboiler duty, representing the process energy demand. The CO_2 capture rate is the percentage of CO_2 removed from the flue gas. Bui et al. [37] highlights two potential ways to calculate the reboiler duty, where the energy supplied to the reboiler is divided by either the CO_2 product flow post-stripping or the difference between the flue gas inlet and clean gas outlet CO_2 flowrates. The energy supplied to the reboiler is the difference between the enthalpy of the inlet utility steam, and saturation enthalpy of the outlet condensed steam [53]. The reboiler duty, in GJ per ton of CO_2 captured, is calculated using:

$$\boldsymbol{R_d = Q_R/(m_{FG_{CO_2}} - m_{CG_{CO_2}})} \quad (8)$$

Where R_d is the reboiler duty (GJ/tCO_2), Q_R is the energy supplied to the reboiler (MJ/h), $m_{FG_{CO_2}}$ is the mass flowrate of the CO_2 in the flue gas (kg/h) and $m_{CG_{CO_2}}$ is the mass flowrate of CO_2 in the cleaned gas (kg/h). Over the duration of the simulation, the reboiler duty can be calculated for that instance as a continuous calculation. Alternatively, averages for the reboiler duty and the total quantity of CO_2 removed per the time frame can be used to determine the overall energy demand for a given operation.

5. Results

The results section includes model validation using steady-state and dynamic data from the literature, and a case study looking at different operating scenarios for transient small-scale PCC operation.

5.1. Steady-State and Dynamic Validation

Although a large number of pilot plant data is openly available, the number of dynamic operating data limited. Dynamic model validation against steady-state data is beneficial [54, 55, 56, 57, 58], however, it doesn't automatically correspond to dynamic operation. Several studies have validated dynamic models against dynamic pilot scale plant data [59, 60, 61] and demonstration scale plant data [62, 63]. Tait et al. [30] presented pilot-scale results for flexible gas-PCC operation. Their investigation tested five different dynamic capture plant scenarios: start-up, shutdown, capture plant decoupling, reboiler decoupling, and frequency response. A summary of the baseload operating conditions is shown in Table 3. The capture plant uses 30.16 wt.% MEA, and the flue gas is representative of a GT with 4.27 vol.% CO_2.

Table 3: Key process parameters for the baseload operating scenario from Tait et al. [30]

Process Parameter		**Value**
Absorber	Packing material	Sulzer Mellapak 250.X
	Packing height (m)	6.92
	Packing diameter (mm)	158.00
Stripper	Packing material	Sulzer Mellapak 500.X
	Packing height (m)	5.00
	Packing diameter (mm)	350.00
Flue gas flowrate (Nm^3/h)		120.50
Flue gas temperature (°C)		46.14
Flue gas CO_2 concentration (vol.%)		4.27
Solvent flowrate (L/h)		344.40
Solvent temperature into absorber (°C)		40.05
Solvent temperature into stripper (°C)		104.07
L/G ratio (L/m^3)		2.86
Steam flowrate to reboiler (kg/h)		19.50
Steam pressure (bar)		4.00
Stripper pressure (bar)		1.80
Reboiler Duty (GJ/tCO_2)		3.96
Lean loading (mol CO_2/mol MEA)		0.232
Rich Loading (mol CO_2/mol MEA)		0.345

The choice of packing material dictates the hydraulic parameters required to calculate the pressure drop, and the coefficients required in the mass transfer correlations. Table 4 shows the values used in this study, based off the values from Billet and Schultes [50] for Mellapak 250Y. For the stripping column the specific area is 500 m^2/m^3.

Table 4: Packing specific parameters

Packing Specific Parameter	Value
Void Fraction	0.970
Specific Area (m^2/m^3)	250
Nominal Size (mm)	50
Loading Point Coefficient	3.157
Flooding Point Coefficient	2.464
Liquid Holdup Coefficient	0.554
Pressure drop Coefficient	0.292

To accurately assess the model's capability under different transient operating scenarios, both the start-up and shutdown experiments are used for validation, these aspects of full-cycle operation will also be included in the case studies in Section 5.2.1. In Tait et al. [30], during the shutdown procedure the flue gas and solvent flowrates are simultaneously decreased over 16 minutes to 40% baseload, then further decreased to 30% baseload over the next 4 minutes. The steam flowrate to the reboiler, is decreased to 0% load in the first 10 minutes. At 20 minutes the flue gas is flowrate is dropped to 0% baseload. The ramp rates in Tait et al. [30] were taken from a Siemens STG5-4000F. For the start-up procedure, the steam flowrate and gas flowrates start at 0% baseload, whilst the solvent flowrate remains at 30% baseload. Over 5.25 minutes the gas flowrate is increased to 30% baseload, and then both gas and solvent flowrates are increased simultaneously to maintain a constant L/G ratio. A more detailed explanation of the operating procedures can be found in Tait et al. [30]. Figure 6 and Figure 5 show a comparison of the flowrates during both operating scenarios. Due to model constraints 0% baseload is un-obtainable, therefore, as close to 0% as possible is achieved (<1% for all flowrates).

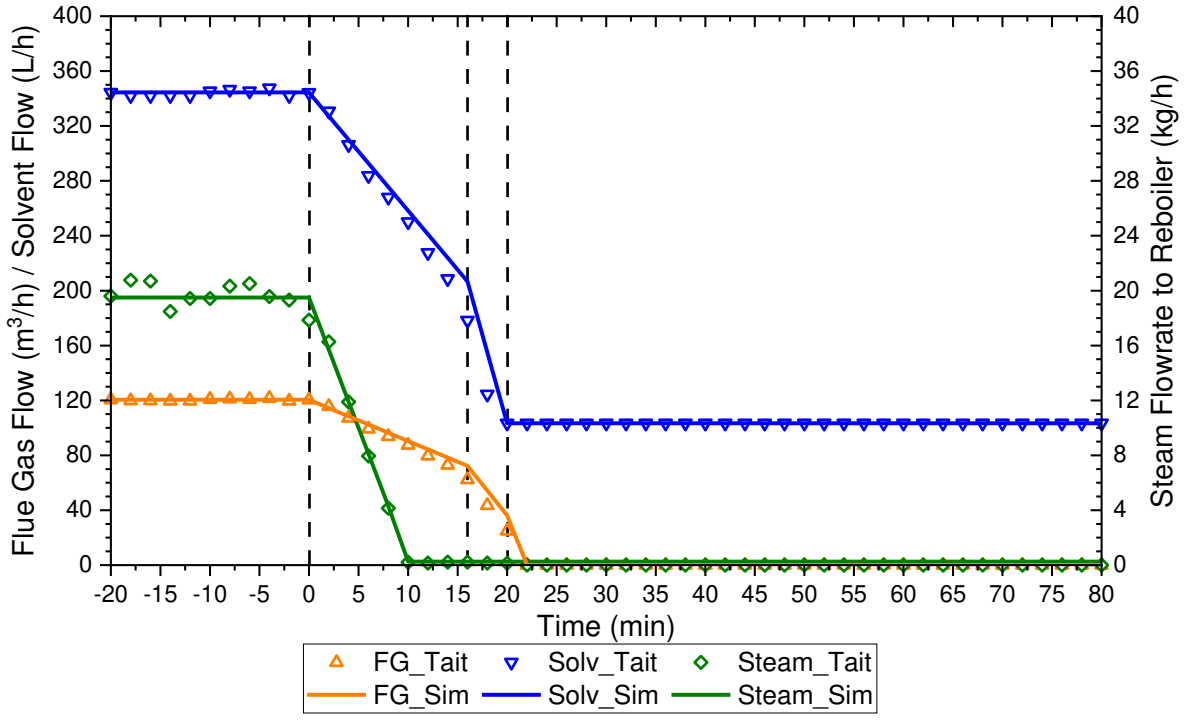

Figure 5: Comparison of flue gas, solvent and steam flowrates during the shutdown scenario

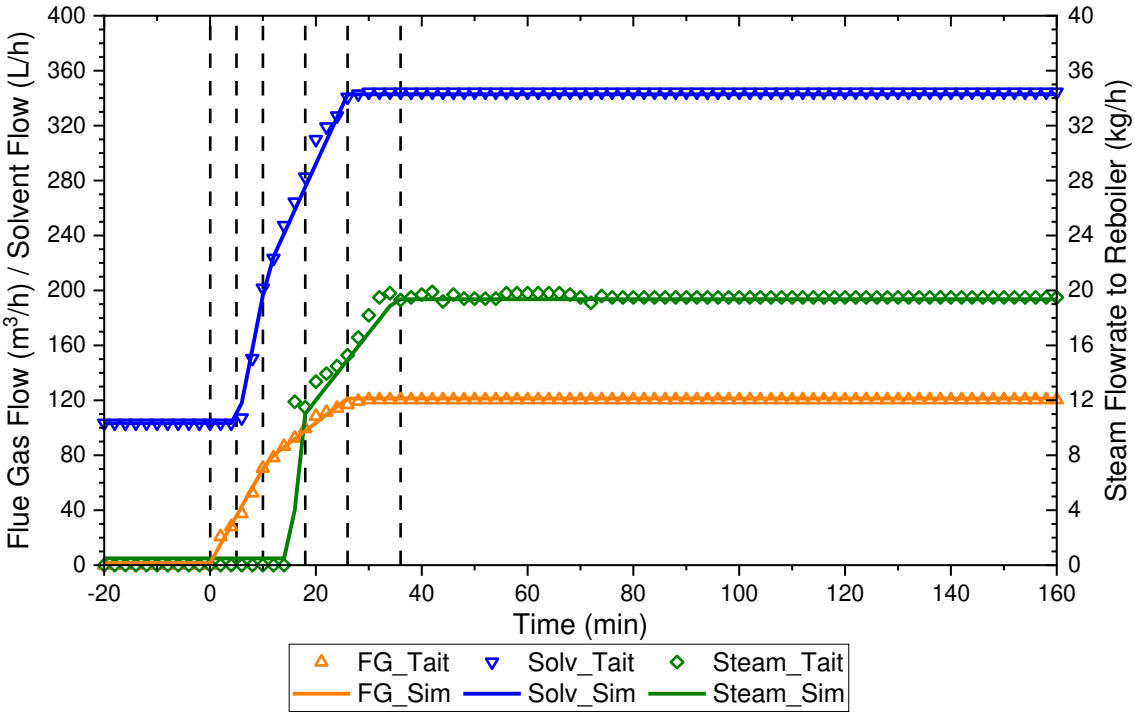

Figure 6: Comparison of flue gas, solvent and steam flowrates during the start-up scenario

Tontiwachwuthikul et al. [64] concluded that absorption column model validation should be performed using concentration and temperature profiles, instead of top and bottom conditions, as the mass/heat transfer has a complex relationship with the column temperature. The temperature profile is indicative of the reactions occurring in the column, and as a result it is directly linked to the capture rate. The absorber temperatures profiles at 0 and 20 minutes are shown in Figure 7, highlighting the steady-state and dynamic capabilities respectively.

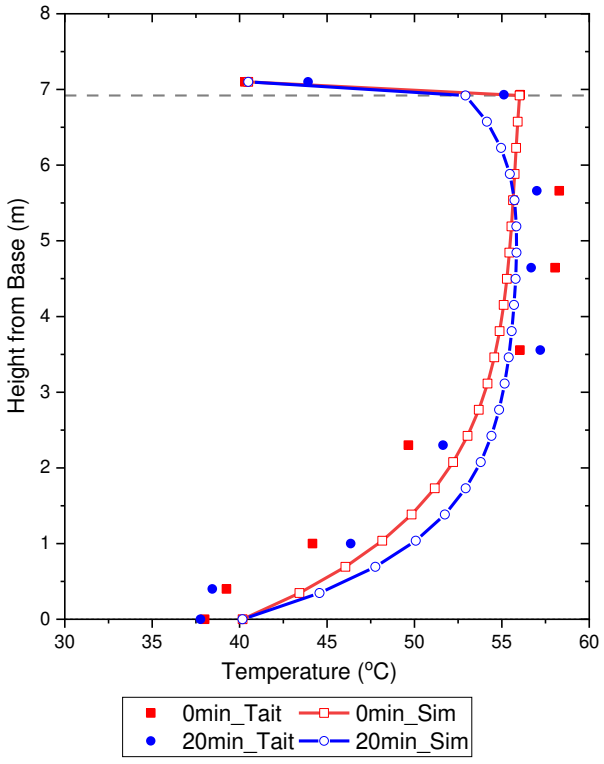

Figure 7: Absorber temperature profile comparison for the shutdown scenario

The top of the column is at 6.92 m, the reading at 7.1m is the inlet solvent stream. In the initial steady state region (0 min) the temperature is the same as the input parameter. However, this temperature decreases as the scenario advances in time. This difference is not accounted for within the current model, as the inlet absorber solvent temperature is a set model input. Kvamsdal and Rochelle [65] describes and analyses a phenomenon called the temperature bulge, which is dependent on column parameters such as: packing height, CO_2 concentration, choice of solvent and L/G ratio. The temperature bulge in each one of the simulations is in the correct location but the magnitude of the temperature bulges deviates by a maximum of 4.85 and 2.28°C at 0 minutes and 20 minutes respectively. The model overall under predicts the temperature profile. As mentioned previously, this is due to the solvent inlet temperature decreasing over time, causing the overall magnitude of the temperature profile to be higher in the model.

Figure 8 and Figure 9 show the dynamic comparison of the capture rate and CO_2 loadings during the dynamic shutdown and start-up scenarios, respectively. During the steady-state operation in the shutdown scenario, the predicted rich- and lean-loadings are 0.333 and 0.218 mol CO_2/mol MEA respectively, which are within the errors indicated by Tait et al. [30]. However, both values are lower than the baseload values shown in Table 3. The specific reboiler duty is calculated by dividing the heat duty of the reboiler by the quantity of CO_2 captured, the predicted value is 4.33 GJ/tCO_2. Tait et al. [30] does not specify the size of the reboiler or condenser, therefore, equipment sizes had to be calculated based off the utility flowrates, resulting in the predicted value for the reboiler duty being 8.54% higher. During the steady-state operation in the start-up procedure the rich- and lean loadings are 0.286 and 0.236 mol CO_2/mol MEA respectively, within the error bars stated by Tait et al. [30]. Therefore, the model accurately simulates steady-state operation.

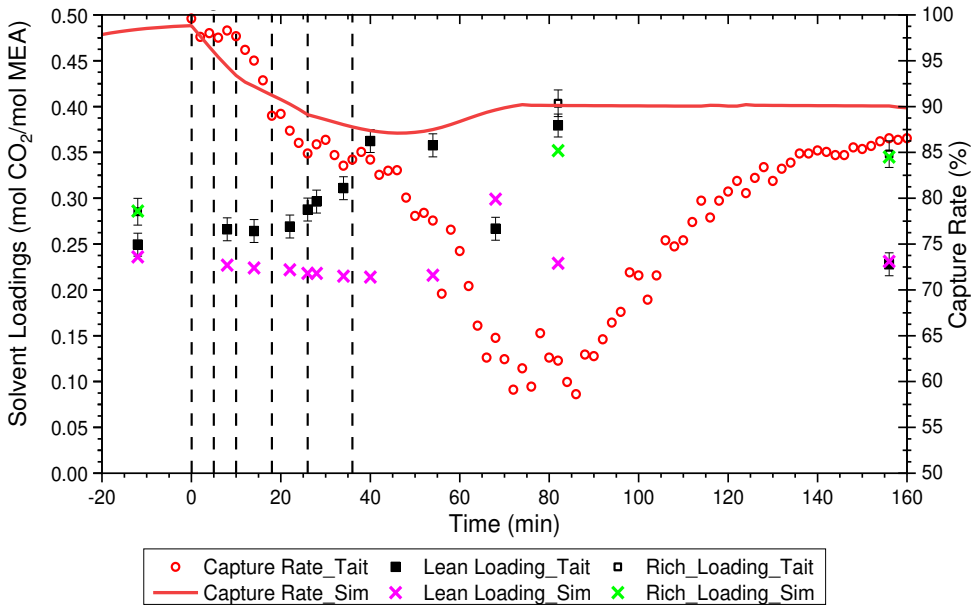

Figure 8: Dynamic comparison of the capture rate and solvent loadings during the shutdown scenario

During dynamic operation, the shutdown scenario capture rate predicated by the model follows the same trajectory as the experiment, the major deviation occurs when the steam flowrate to the reboiler is 0 kg/h at t=10 minutes. At this point the gradient of the capture rate in the experiment increases, whereas the model remains on the same course, until the flue gas and solvent flowrate ramp rates are changed at t=16 minutes. At this time the model under predicts the capture rate by 2.44%, which is the largest difference exhibited throughout this scenario. At the end of the dynamic operation, at t=20 minutes, the predicted capture rate is 1% lower

than presented in Tait et al. [30]. Over the entire shutdown scenario, the rich- and lean-loadings predicted by the model are lower than the experiment, although they follow a similar profile. A similar problem occurs in the start-up scenario indicating the working fluid contains a lower percentage of CO_2. Further research is required on the desorption unit to determine the reason for this lower loading. In the start-up scenario, the initial and end loadings predicted by the model are within the error bars presented in Tait et al. [30].

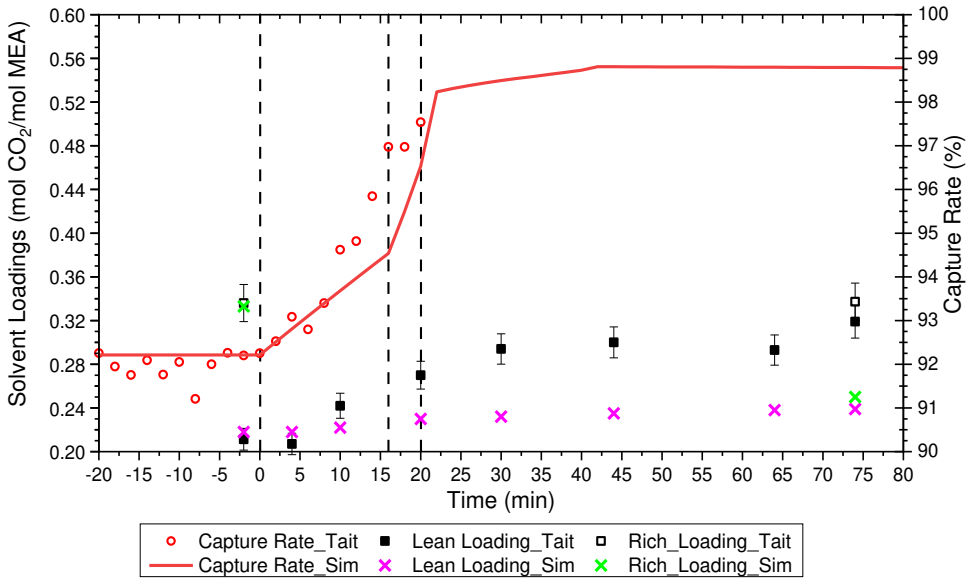

Figure 9: Dynamic comparison of the capture rate and solvent loadings during the start-up scenario

As mentioned previously, due to the time taken for real-world systems to return to steady-state following a perturbation, the differences in the loadings during the middle of the operation are expected to be greater than at the start and end. Alongside the capture rate curve, this highlights the model returns to steady-state at a faster rate than the experiment. It is worth noting that the experiment did not incorporate rich-solvent heating (used to simulate the temperature increase caused by the solvent cross-over heat exchanger) until t=60 minutes. Consequently, the desorber solvent inlet temperature increases to 50-60°C higher than the baseload experiment, causing the lean loading (recorded after the desorption step) to increase gradually. This explains the larger lean loading deviation between t=0 to 60 minutes.

5.2. Case Study

The model is scaled to handle 33.8 kg/s of flue gas, whilst maintaining the same L/G ratio from Tait et al. [30], equating to 83.04 kg/s of solvent flow with 30.16 wt. % MEA. The model is designed in such a way that the absorber solvent MEA concentration is maintained at this concentration through the 'Make_up' unit shown in Figure 4. Using the method described in Section 4, the main calculated process parameters for the scaled model are shown in Table 5 alongside the steady-state model output. The scaled values for the absorber and stripping columns represent non-optimised values to attain similar capture rate and loadings as the baseload conditions presented in Tait et al. [30]. The solvent crossover heat-exchanger heat transfer area is the value required to ensure the rich solvent temperature entering the stripping column is 104.07°C. The calculated reboiler steam flowrate achieves the same temperature (at Measurement002 on Figure 4) as the validation simulation. The flue gas flowrate is 33.80 kg/s or 104,530 Sm^3/h, similar in scale to the TCM capture plant which can process 60,000 Sm^3/h of flue gas. The TCM plant absorber packing height is 24m with a column cross sectional area of 3.55x2m, the stripping column is smaller with a packing height of 8m and a diameter of 1.33m [37]. The demonstration facility also incorperates a solvent crossover heat-exchanger with an area of 308m^2 [63].

Table 5: Scaled model parameters

Process Parameter	**Value**
Flue Gas Flowrate (kg/s)	33.80
Absorber Inlet Solvent Flowrate (kg/s)	83.04
Absorber Column Height (m)	18.5
Absorber Column Diameter (m)	8.2
Stripper Column Height (m)	15.5
Stripper Column Diameter (m)	4.5
Solvent Crossover Heat-exchanger Area (m^2)	448.45
Reboiler Volume (m^3)	5.00
Condenser Volume (m^3)	5.00
Reboiler Steam Flowrate (kg/s)	3.75
Steady-state model output	
Lean-loading (mol CO_2/mol MEA)	0.2366
Rich-loading (mol CO_2/mol MEA)	0.3287
Capture Rate (%)	92.48
Reboiler Duty (GJ/tCO_2)	3.93

5.2.1. Operating Scenarios

The dynamic changes for the flue gas, solvent and reboiler steam flowrates are shown in Figure 10. In Scenario A, only the flue gas flow entering the absorber is ramped, see Figure 3 for ramp times and percentage changes in flowrate. Each subsequent scenario includes the manipulation of an additional flowrate, i.e. the solvent entering the absorber, or the steam used to heat the reboiler. In reality the ramping rates of the steam supply to the reboiler will be higher, however, for the purpose of determining the effects each variable has, it follows the same ramp rates as the flue gas and the solvent flows. It is worth noting that due to model constraints the streams cannot converge to 0 kg/s, therefore, all flowrates are decreased to a minimum of 1% baseload.

Figure 10 also highlights the capture rate for each scenario during the five-hour dynamic operation. Over the course of each operating Scenario A, B, C and Baseload the capture rate is 1.08, 0.73, 1.2% and 0.81% points lower, respectively, compared to the steady-state value of 92.48% in Table 5. This is a result of including the start-up, ramping and shutdown procedures; over the entire simulation this drop is insignificant and the time-averaged capture rates are around 90% for all scenarios. The largest capture rate drops are during the periods directly after 70% or 50% load. This is a result of the transition time, showing the new set of parameters have not reached steady-state. The decrease in capture rate during each new load is less than 2%, similar to the rate changes published in Bui et al. [37] when the L/G ratio is kept constant (Scenario B and C). It is worth mentioning that in Bui et al. [37] during the dynamic operation each new set of process conditions are maintained for several hours, re-reaching steady-state or near steady-state conditions. The decrease in capture rate is a result of the lean-loading increasing by 3.28% between t=8 to 300 minutes in the Baseload scenario. As more CO_2 is entrained in the solvent, less CO_2 can be absorbed. Interestingly, when returning to full load the capture rates continue their original trajectory, and the start-up/shutdown procedures balance each other out.

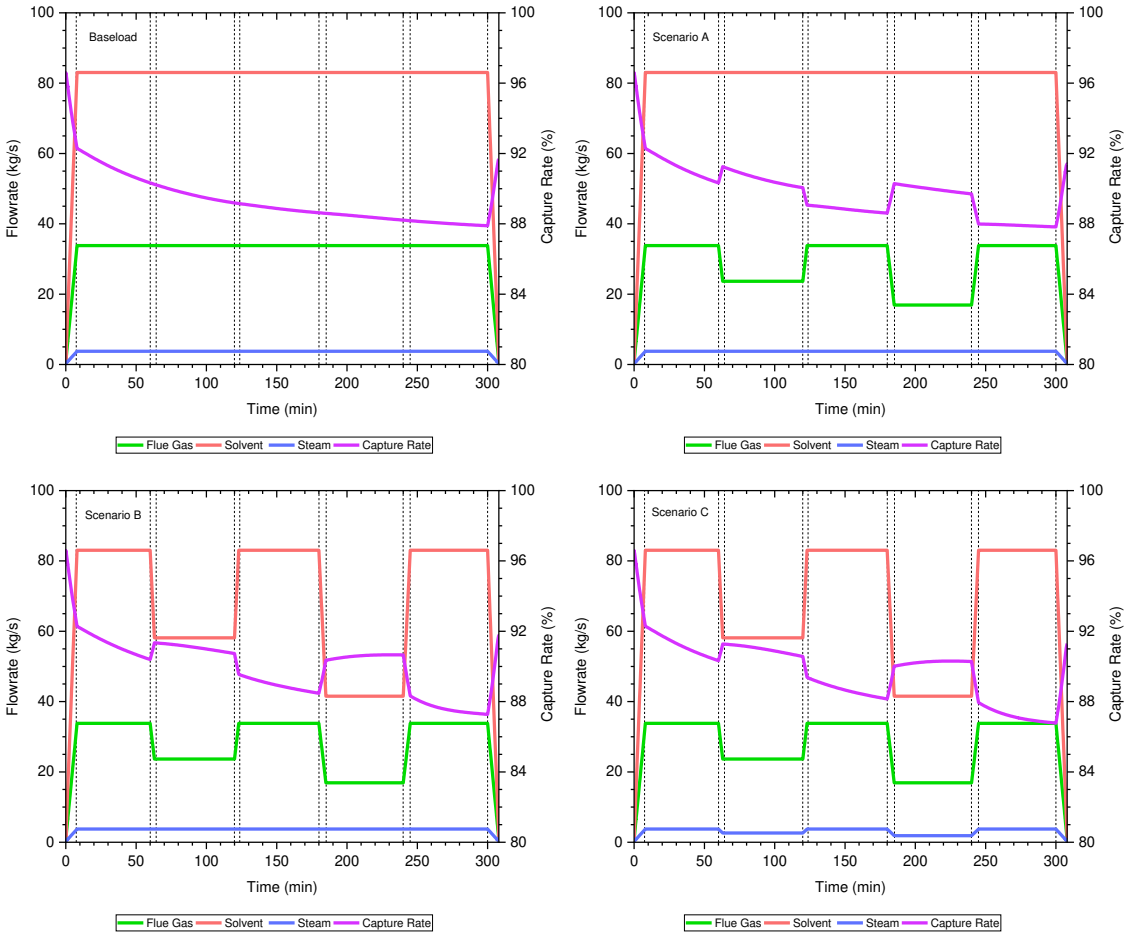

Figure 10: Flowrate changes and capture rate profile for each operating scenario

Figure 10 shows the one-hour operating cycle is not long enough for the capture rate to level out and stabilise. The time-averaged capture rate is 89.81, 90.01, 89.75 and 89.35% in Scenario A, B, C and the Baseload, respectively. In Scenario A the increase in capture rate is a result of a higher L/G ratio, as more solvent is available to absorb CO_2. Interestingly, this increase is also shown in Scenario B and C, indicating the lower flowrates through the column also increase the capture efficiency. Although the capture rate changes seem small and within normal plant operation guidelines, the simulations show the highly transient operation, i.e. alternating between partial and full loads every hour, is beneficial in delivering a time-averaged capture rate around 90%.

During the transition from 50% to 100% between t=240 to t=245 minutes, Scenario B and C exhibit the largest capture rate drop: 1.89% in both cases. This is also highlighted in Figure 11, which illustrates the bulk vapour temperature profiles for each scenario. With Scenario B and C exhibiting more prolific temperature drops at t=240 minutes. The 3-D temperature profiles show Scenario A and the Baseload scenario remain reasonably constant throughout the simulation. However, the top section of the column, between 12 to 18.5m, the temperature increases by 4K over the course of the simulating. This results in more water evaporation and less CO_2 absorption. The temperature drops following the temperature spikes in Scenario B and C at t = 60, 180, and 300 minutes, indicates a change in solvent flowrate and leads to an increase in capture rate.

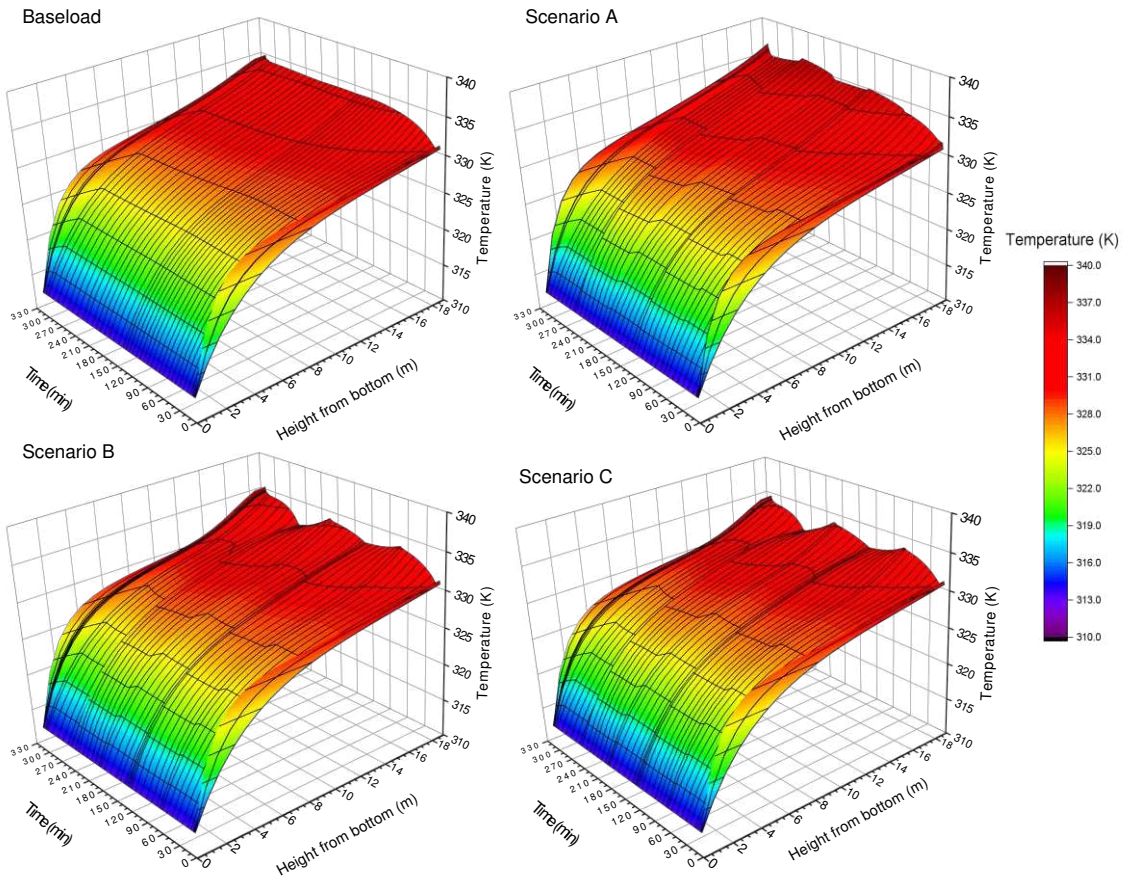

Figure 12: Absorber bulk vapour temperature profile in each scenario

One of the key challenges with using amine solvents for CO_2 capture is oxidative and thermal degradation. Oxidative degradation is a result of the O_2 content in flue gas, this is not analysed in the study. Thermal degradation is a result of the high temperatures and pressures in the stripping column, hence the limitation of 120°C [66]. As shown in Figure 12 this value is not exceeded at any point in the simulation, and Moser et al. [67] showed minimal thermal degradation at 120°C during the 18 month test campaign at RWE's pilot-scaled capture plant in Niederaussem, Germany.

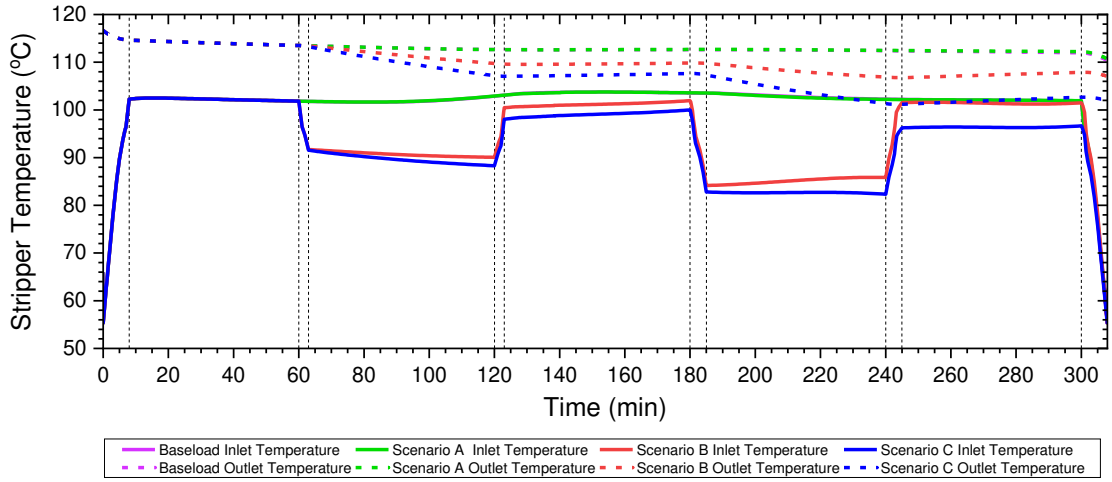

Figure 11: Stripping column inlet and outlet temperatures during each scenario

Interestingly, the inlet stripper temperature directly correlates to the flowrate changes, shown more so in Scenario B and C as the magnitude of change is greater. Nevertheless, the rapid temperature and pressure transitioning influences the lean-loading. Figure 13 shows the lean and rich loading throughout each dynamic scenario. The steady-state baseload lean-loading is 0.237 mol CO_2/mol MEA, the rich-loading is 0.329 mol CO_2/mol MEA and the calculated reboiler duty is 3.93 GJ/tCO_2, within the 3.6-4 GJ/tCO_2 range specified in Bui et al. [12]. The steady-state values are not presented in Figure 13 as the results shown begin with the start-up operation. For the Baseload and Scenario A simulations the lean-loading remains reasonably constant post start-up and pre shutdown. This results from a constant solvent to steam (S/S) ratio. In Scenario B, the smaller solvent flowrate at low load and lower S/S value, means more energy is supplied per unit of rich-solvent. Enabling more CO_2 to be stripped, causing the lean loading to decrease between t=60 to 120 minutes, and t=180 to 240 minutes. Whereas in Scenario C the lean-loading increases due to the drop in steam supplied to the reboiler, increasing the S/S ratio and recuding the enegry avaiable to strip the CO_2. Due to the rapid transitioning, the lean-loading levels do not stabilise in Scenario B and C. Jin et al. [13] explains the effects the lean-loading has on the reboiler duty for the conventional amine-absorption process, and showed a minimum reboiler duty of 3.472 GJ/tCO_2 at 0.2 mol CO_2/mol MEA lean-loading, similar to the results in this paper.

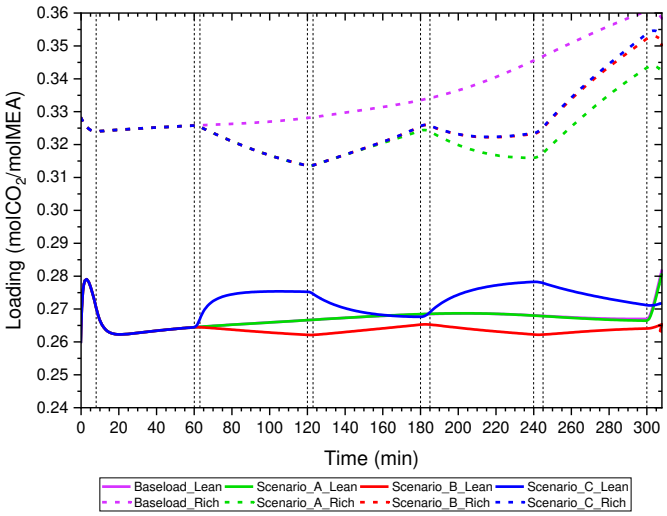

Figure 13: Lean and rich loading throughout each dynamic scenario

Table 6 highlights the percentage differences between the loadings from t=0 to t=308 minutes. The flexible operating scenarios provide a greater control of process parameters compared to the Baseload, which exhibits the greatest overall changes in both rich- and lean-loading, hence the lowest time-averaged capture rate. As the capture rate decreases, theoretically the rich-loading should decrease as well as less CO_2 is absorbed. However, the CO_2 mass fraction in the rich-solvent stream increases due a greater quantiy of water evaporating in the column. The rich-loading is not necessarily a good indicator of the effectivenes of the process.

The transient operation aids in counteracting the long transition periods, which as Bui et al. [37] explains takes up to 114 minutes to re-reach steady state in a large-scale PCC system. In this study the Baseload operation does not reach steady-state until the end of the five hour operation, longer than that reported in Montañés et al. [34] and Bui et al. [37]. This is due to the larger flowrates and equipment sizes, increasing solvent circulation time. As well as non-optimised equipment geometries, which have been scaled to produce the same key operating parameters as the pilot faciltiy, in reality the larger systems will not have identical performance.

Table 6: Loading changes over the entire simulation for each scenario

Scenario	Lean-loading (mol CO_2/mol MEA)			Rich-loading (mol CO_2/mol MEA)		
	t=0 min	t=308 min	%Difference	t=0 min	t=308 min	%Difference
Baseload	0.263	0.282	7.22	0.328	0.358	9.15
A	0.263	0.281	6.84	0.328	0.341	3.96
B	0.263	0.263	0	0.328	0.350	6.71
C	0.263	0.272	3.42	0.328	0.353	7.62

Figure 14 shows the reboiler duties for each scenario, based on the energy supplied to the reboiler via the pressurised steam, and the quantity of CO_2 captured over the five-hour operation. Scenario B captures the most CO_2 out of the flexible operating scenarios. During the operation it captures 26kg more than Scenario C and 67kg more than Scenario A. Although this seems insignificant, assuming an annual operating time of 230 hours as explained in Section 2, the annual difference in CO_2 captured between Scenario B and A is 3.08 tonnes. Interestingly, there is a potential energy saving when manipulating the reboiler steam flowrate in accordance to the GT load. Scenario C shows an 18.22% energy saving compared to Scenario A, with a reboiler duty of 3.95 GJ/tCO_2. This is 0.01 GJ/tCO_2 lower than the Baseload scenario, where the capture plant is operated at full load for the entirety of the five-hour operation. This is within the accuracy of model, highlighting there are no negative energy related effects of transient operation. Further research is required to determine the potential savings associated with manipulating the reboiler steam flowrate, and to develop an optimal operating strategy to minimise energy losses.

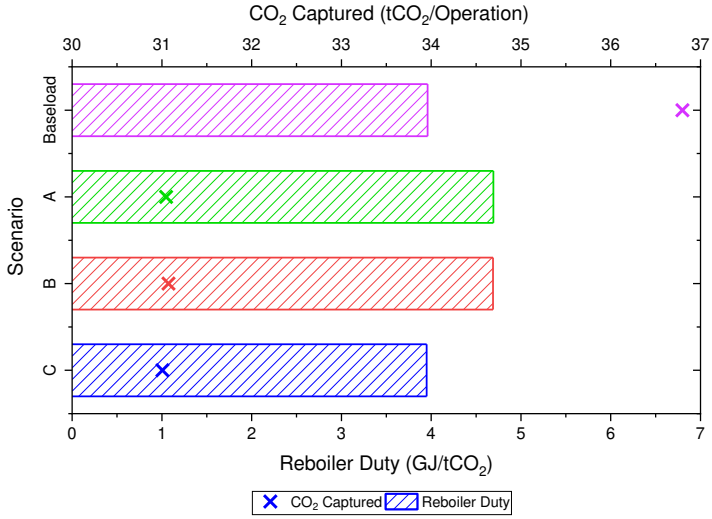

Figure 14: Reboiler duty and quantity of CO_2 captured during each operating scenario

Figure 15 shows the pressure drop in the reboiler for each scenario, and as expected Scenario C shows the greatest decline in reboiler pressure, similar to the outlet stripper temperatures shown in Figure 12. Compared to the initial reboiler pressure of 1.8 bar, the overall pressure drop is 15.49, 26.70, 41.24, and 19.37% for Scenario A, B, C and the Baseload respectively. The pressure drop and the consequent loss in purity has an effect on the compression system required to pressurise the CO_2 for pipeline transportation and storage [68, 69]. More information on the effects of transient CO_2 production on a compression system can be found in Spitz et al. [23] and Mechleri, et al. [25].

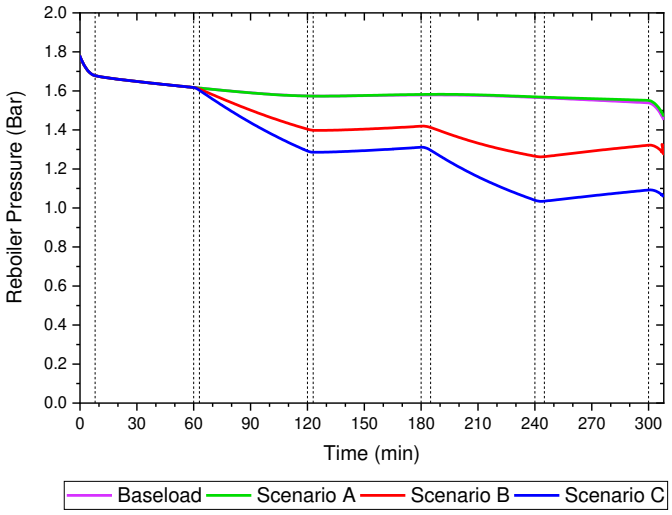

Figure 15: Reboiler pressure drop over each dynamic scenario

6. Conclusion

Complex energy systems with a range of generation technologies require secure, reliable and flexible power. The fast ramping capabilities of modern gas turbines can be used as dispatchable generation, in order to combat the intermittency issues of renewable energy. Accompanied with CCUS, quick-starting gas turbines can play a vital role in decarbonising the energy sector. This paper shows the development and validation of a rate-based CO_2 absorption model, using the benchmark 30 wt.% MEA solvent. The typical transient operation of fast-ramping OCGT generation is shown, as well as how these fluctuations in exhaust flow (due to changes in power output) effect the capture rate and other key process indicators.

OCGT generation typically comes on the GB electricity system in the evening on cold winter days, corresponding to peak system demand. On average each operating cycle is five hours, therefore, this is the time frame used in this study to evaluate the transient performance of amine-based PCC. The results show the capture rate drop is less severe in the flexible operating scenarios, as alternating between full and partial loads in a short period of time does not allow CO_2 loadings to stabilise. Therefore, transient behaviour aids in delivering a time-averaged capture rate above 90%. Reducing the reboiler steam flowrate in accordance with the flue gas flowrate delivers a 0.01 GJ/tCO_2 lower reboiler duty than the Baseload scenario. Not a significant reduction, however, this shows there are no negative effects on energy demand due to transient operation. Additional research is required to find an optimal operating strategy to further minimise the energy penalty and deliver improved process performance.

Several flexibility studies discuss the use of reboiler steam being redirected to the steam turbine, increasing the power output of the plant for economic or frequency response situations. An OCGT plant does not have the steam turbine and therefore is not suitable for this type of transient behaviour. However, the excess thermal energy in the exhaust can be used to heat the steam required for the reboiler. Further research is required to determine the feasibility of integrating the waste thermal energy from an OCGT plant into a PCC plant; to minimise the PCC energy penalty without hindering the OCGT electrical power output.

7. Acknowledgements

This work is funded by the Engineering and Physical Sciences Research Council (EPSRC) Centre for Doctoral Training in Carbon Capture and Storage and Cleaner Fossil Energy (reference: EP/L016362/1), and Drax Group Plc. The author would like to acknowledge the support of the Royal Academy of Engineering through the Industrial Fellowship (reference: IF\192046).

8. References

[1] C. F. Heuberger and N. Mac Dowell, "Real-World Challenges with a Rapid Transition to 100% Renewable Power System," *Joule,* vol. 2, no. 3, pp. 367-370, 2018.

[2] M. Huber, D. Dimkova and T. Hamacher, "Integration of wind and solar power in Europe: Assessment of flexibility requirements," *Energy,* vol. 69, pp. 236-246, 2014.

[3] G. Wynn and D. Schlissel, "Electricity-Grid Transition in the U.K.: As Coal-Fired Generation Recedes, Renewables and Reliable Generation Can Fill the Gap," The Institute for Energy Economics and Financial Analysis, 2017.

[4] R. Lee, S. Homan, N. M. Dowell and S. Brown, "A closed-loop analysis of grid scale battery systems providing frequency response and reserve services in a variable inertia grid," *Applied Energy,* vol. 236, pp. 961-972, 2019.

[5] Parsons Brinckerhoff, "Technical Assessment of the Operation of Coal & Gas Fired Plants," Department of Energy and Climate Change, London, 2014.

[6] S. Brown, K. S. Campbell, G. Gadikota, A. Howe and N. M. Dowell, "CCS Forum Report," IChemE, London, 2016.

[7] Agora Energiewende, "Flexibility in thermal power plants," Agora Energiewende, Berlin, 2017.

[8] MHPS, "Gas Turbines H-25 Series," 2019. [Online]. Available: https://www.mhps.com/products/gasturbines/lineup/h25/index.html. [Accessed 20 April 2019].

[9] GE, "TM2500 POWER PLANTS," General Electric Power , 2019.

[10] Siemens, "Gas Turbine Portfolio Brochure," Siemens, Munich, 2019.

[11] Solar Turbines, "Product Handbook for Power Generation," Solar Turbines, 2019.

[12] M. Bui, C. S. Adjiman, A. Bardow, E. J. Anthony, A. Boston, S. Brown, P. S. Fennell, S. Fuss, A. Galindo, L. A. Hackett, J. P. Hallett, H. J. Harzog, G. Jackson, J. Kemper, S. Krevor, G. C. Maitland, M. Matuszewski, I. S. Metcalfe, C. Petit, G. Puxty, J. Reimer, D. Reiner, E. Rubin, S. Scott, N. Shah, B. Smit, J. P. Trusler, P. Webley, J. Wilcox and N. Mac Dowell, "Carbon capture and storage (CCS): the way forward," *Energy & Environmental Science,* vol. 11, no. 5, pp. 1062-1176, 2018.

[13] H. Jin, P. Liu and Z. Li, "Energy-efficient process intensification for post-combustion CO2 capture: A modeling approach," *Energy,* vol. 158, pp. 471-483, 2018.

[14] Z. Zhang, T. N. Borhani and A. G. Olabi, "Status and perspective of CO2 absorption process," *Energy,* vol. 205, p. 118057, 2020.

[15] H.-T. Oh, Y. Ju, K. Chung and C.-H. Lee, "Techno-economic analysis of advanced stripper configurations for post-combustion CO2 capture amine processes," *Energy,* vol. 206, p. 118164, 2020.

[16] S.-Y. Oh and J.-K. Kim, "Operational optimization for part-load performance of amine-based post-combustion CO2 capture processes," *Energy,* vol. 146, pp. 57-66, 2018.

[17] IEAGHG, "Valuing Flexibility in CCS Power Plants," IEA Greenhoouse Gas R&D Programme, Cheltenham, 2017.

[18] R. Domenichini, L. Mancuso, N. Ferrari and J. Davison, "Operating Flexibility of Power Plants with Carbon Capture and Storage (CCS)," *Energy Procedia,* vol. 37, pp. 2727-2737, 2013.

[19] C. F. Heuberger, I. S. N. Shahbc and N. M. Dowell, "Quantifying the value of CCS for the future," *Energy & Environmental Science,* vol. 9, pp. 2497-2510, 2016.

[20] N. Mac Dowell and Staffell, "The role of flexible CCS in the UK's future energy system," *International Journal of Greenhouse Gas Control,* vol. 48, no. 2, pp. 327-344, 2016.

[21] D. L. Oates, P. Versteeg, E. Hittinger and P. Jaramillo, "Profitability of CCS with flue gas bypass and solvent storage," *International Journal of Greenhouse Gas Control,* vol. 27, pp. 279-288, 2014.

[22] E. Sanchez-Fernandez, M. Sanchez del Rio, H. Chalmers, P. Khakharia, E. L. V. Goetheer, J. Gibbins and M. Lucquiaud, "Operational flexibility options in power plants with integrated post-combustion capture," *International Journal of Greenhouse Gas Control,* vol. 48, pp. 275-289, 2016.

[23] T. Spitz, A. G. Díaz, H. Chalmers and M. Lucquiaud, "Operating flexibility of natural gas combined cycle power plant integrated with post-combustion capture," *International Journal of Greenhouse Gas Control,* vol. 88, pp. 92-108, 2019.

[24] M. D. Wilkes and S. Brown, "Evaluating the Transient Operation of PCC for Fast Response Gas Turbines in a Future Low-Carbon Energy System," *Computer Aided Chemical Engineering,* vol. 48, pp. 157-162, 2020.

[25] E. Mechleri, A. Lawal, A. Ramos, J. Davison and N. Mac Dowell, "Process control strategies for flexible operation of post-combustion CO2 capture plants," *International Journal of Greenhouse Gas Control,* vol. 57, pp. 14-25, 2017a.

[26] X. Wu, M. Wang and K. Y. Lee, "Flexible operation of supercritical coal-fired power plant integrated with solvent-based CO2 capture through collaborative predictive control," *Energy,* vol. 206, p. 118105, 2020a.

[27] E. Mechleri, P. S. Fennell and N. Mac Dowell, "Optimisation and evaluation of flexible operation strategies for coal-and gas-CCS power stations with a multi-period design approach," *International Journal of Greenhouse Gas Control,* vol. 59, pp. 24-39, 2017b.

[28] R. M. Montañés, M. Korpås, L. O. Nord and S. Jaehnert, "Identifying Operational Requirements for Flexible CCS Power Plant in Future Energy Systems," *Energy Procedia,* vol. 86, pp. 22-31, 2016.

[29] S. Giorgetti, A. Parente, L. Bricteux, F. Contino and W. D. Paepe, "Optimal design and operating strategy of a carbon-clean micro gas turbine for combined heat and power applications," *International Journal of Greenhouse Gas Control,* vol. 88, pp. 469-481, 2019.

[30] P. Tait, B. Buschle, I. Ausner, P. Valluri, M. Wehrli and M. Lucquiaud, "A pilot-scale study of dynamic response scenarios for the flexible operation of post-combustion CO2

capture," *International Journal of Greenhouse Gas Control,* vol. 48, no. 2, pp. 216-233, 2016.

[31] ELEXON, "Balancing Mechanism Reporting Service (BMRS)," 2019. [Online]. Available: https://www.bmreports.com. [Accessed 1 November 2019].

[32] A. Mangiaracina, L. Zangrilli, L. Robinson, H. M. Kvamsdal and P. V. Os, "OCTAVIUS: Evaluation of Flexibility and operability of Amine Based Post Combustion CO2 Capture at the Brindisi Pilot Plant," *Energy Procedia,* vol. 63, pp. 1617-1636, 2014.

[33] M. Bui, I. Gunawan, V. Verheyen, P. Feron and E. Meuleman, "Flexible operation of CSIRO's post-combustion CO2 capture pilot plant at the AGL Loy Yang power station," *International Journal of Greenhouse Gas Control,* vol. 48, no. 2, pp. 188-203, 2016.

[34] R. M. Montañés, N. E. Flø and L. O. Nord, "Experimental results of transient testing at the amine plant at Technology Centre Mongstad: Open-loop responses and performance of decentralized control structures for load changes," *International Journal of Greenhouse Gas Control,* vol. 73, pp. 42-59, 2018.

[35] P. Tait, B. Buschle, K. Milkowski, M. Akram, M. Pourkashanian and M. Lucquiaud, "Flexible operation of post-combustion CO2 capture at pilot scale with demonstration of capture-efficiency control using online solvent measurements," *International Journal of Greenhouse Gas Control,* vol. 71, pp. 253-277, 2018.

[36] N. Mac Dowell and N. Shah, "Optimisation of Post-combustion CO2 Capture for Flexible Operation," *Energy Procedia,* vol. 63, pp. 1525-1535, 2014.

[37] M. Bui, N. E. Flø, T. Cazenove and N. M. Dowell, "Demonstrating flexible operation of the Technology Centre Mongstad (TCM) CO2 capture plant," *International Journal of Greenhouse Gas Control,* vol. 93, p. 102879, 2020.

[38] J.-M. Bellas, K. N. Finney, M. E. Diego, D. Ingham and M. Pourkashanian, "Experimental investigation of the impacts of selective exhaust gas recirculation on a micro gas turbine," *International Journal of Greenhouse Gas Control,* vol. 90, p. Article 102809, 2019.

[39] A. Chikukwa, N. Enaasen, H. M. Kvamsdal and M. Hillestad, "Dynamic Modeling of Post-combustion CO2 Capture Using Amines–A Review," *Energy Procedia,* vol. 23, pp. 82-91, 2012.

[40] M. Bui, I. Gunawan, V. Verheyen, P. Feron, E. Meuleman and S. Adeloju, "Dynamic modelling and optimisation of flexible operation in post-combustion CO2 capture plants—A review," *Computers & Chemical Engineering,* vol. 61, pp. 245-265, 2014.

[41] X. Wu, M. Wang, P. Liao, J. Shen and Y. Li, "Solvent-based post-combustion CO2 capture for power plants: A critical review and perspective on dynamic modelling, system identification, process control and flexible operation," *Applied Energy,* vol. 257, p. 113941, 2020b.

[42] N. Mac Dowell and N. Shah, "The multi-period optimisation of an amine-based CO2 capture process integrated with a super-critical coal-fired power station for flexible operation," *Computers & Chemical Engineering,* vol. 74, pp. 169-183, 2015.

[43] R. Taylor and R. Krishna, Multicomponent Mass Transfer, New York: John Wiley & Sons, Inc, 1993.

[44] P. Mores, N. Scenna and S. Mussati, "CO2 capture using monoethanolamine (MEA) aqueous solution: Modeling and optimization of the solvent regeneration and CO2 desorption process," *Energy,* vol. 45, no. 1, pp. 1042-1058, 2012.

[45] J. L. Bravo and J. R. Fair, “Generalized correlation for mass transfer in packed distillation columns,” *Industrial & Engineering Chemistry Process Design and Development,* vol. 21, no. 1, pp. 162-170, 1982.

[46] K. Onda, H. Takeuchi and Y. Okumoto, "Mass Transfer Coefficients Between Gas and Liquid Phases in Packed Columns," *Journal of Chemical Engineering Japan,* vol. 1, pp. 56-62, 1968.

[47] E. R. Dugas, "Pilot plant study of carbon dioxide capture by aqueous monoethanolamine, M.S.E. Thesis," University of Texas at Austin, 2006.

[48] PSE, "gCCS Documentation," Process Systems Enterprise Limited, London, 2016.

[49] N. Mac Dowell, F. Llovell, C. S. Adjiman, G. Jackson and A. Galindo, "Modeling the Fluid Phase Behavior of Carbon Dioxide in Aqueous Solutions of Monoethanolamine Using Transferable Parameters with the SAFT-VR Approach," *Industrial & Engineering Chemistry Research,* vol. 49, no. 4, pp. 1883-1899, 2010.

[50] R. Billet and M. Schultes, "Prediction of Mass Transfer Columns with Dumped and Arranged Packings: Updated Summary of the Calculation Method of Billet and Schultes," *Chemical Engineering Research and Design,* vol. 77, no. 6, pp. 498-504, 1999.

[51] N. Mac Dowell, N. J. Samsatli and N. Shah, "Dynamic modelling and analysis of an amine-based post-combustion CO2 capture absorption column," *International Journal of Greenhouse Gas Control,* vol. 12, pp. 247-258, 2013.

[52] R. K. Shah and D. P. Sekulić, Fundamentals of Heat Exchanger Design, New Jersey: John Wiley & Sons, 2003.

[53] L. Faramarzi, D. Thimsen, S. Hume, A. Maxon, G. Watson, S. Pedersen, E. Gjernes, B. F. Fostås, G. Lombardo, T. Cents, A. K. Morken, M. I. Shah, T. d. C. Espen and S. Hamborg, "Results from MEA testing at the CO2 Technology Centre Mongstad: Verification of baseline results in 2015," *Energy Procedia,* vol. 114, pp. 1128-1145, 2017.

[54] H. M. Kvamsdal, J. P. Jakobsen and K. Hoff, "Dynamic modeling and simulation of a CO2 absorber column for post-combustion CO2 capture," *Chemical Engineering and Processing: Process Intensification,* vol. 48, pp. 135-144, 2009.

[55] A. Lawal, M. Wang, P. Stephenson, G. Koumpouras and H. Yeung, "Dynamic modelling and analysis of post-combustion CO2 chemical," *Fuel,* vol. 89, pp. 2791-2801, 2010.

[56] M. T. Luu, N. A. Manaf and A. Abbas, "Dynamic modelling and control strategies for flexible operation of amine-based post-combustion CO2 capture systems," *International Journal of Greenhouse Gas Control,* vol. 39, pp. 377-389, 2015.

[57] F. Rezazadeh, W. F. Gale, M. Akram, K. J. Hughes and M. Pourkashanian, "Performance evaluation and optimisation of post combustion CO2 capture processes for natural gas applications at pilot scale via verified rate-based models," *International Journal of Greenhouse Gas Control,* vol. 53, pp. 243-253, 2016.

[58] L. Prentza, I. P. Koronaki, E. G. Papoutsis and V. D. Papaefthimiou, "Dynamic simulation and parametric sensitivity study in reactive CO2 capture systems – A solvent comparison study," *Thermal Science and Engineering Progress,* vol. 5, pp. 555-567, 2018.

[59] C. Biliyok, A. Lawal, M. Wang and F. Seibert, "Dynamic modelling, validation and analysis of post-combustion chemical absorption CO2 capture plant," *International Journal of Greenhouse Gas Control,* vol. 9, pp. 428-445, 2012.

[60] N. A. Manaf, A. Cousins, P. Feron and A. Abbas, "Dynamic modelling, identification and preliminary control analysis of an amine-based post-combustion CO2 capture pilot plant," *Journal of Cleaner Production,* vol. 113, pp. 635-653, 2016.

[61] M. Bui, P. Tait, M. Lucquiaud and N. Mac Dowell, "Dynamic operation and modelling of amine-based CO2 capture at pilot scale," *International Journal of Greenhouse Gas Control,* vol. 79, pp. 134-153, 2018.

[62] N. Enaasen, L. Zangrilli, A. Mangiaracina, T. Mejdell, H. M. Kvamsdal and M. Hillestad, "Validation of a Dynamic Model of the Brindisi Pilot Plant," *Energy Procedia ,* vol. 63, pp. 1040-1054, 2014.

[63] R. M. Montañés, N. E. Flø and L. O. Nord, "Dynamic Process Model Validation and Control of the Amine Plant at CO2 Technology Centre Mongstad," *Energies,* vol. 10, p. 1527, 2017.

[64] P. Tontiwachwuthikul, A. Meisen and C. J. Lim, "CO2 absorption by NaOH, monoethanolamine and 2-amino-2-methyl-1-propanol solutions in a packed column," *Chemical Engineering Science,* vol. 47, no. 2, pp. 381-390, 1992.

[65] H. M. Kvamsdal and G. T. Rochelle, "Effects of the Temperature Bulge in CO2 Absorption from Flue Gas by Aqueous," *Industrial & Engineering Chemistry Research,* vol. 47, no. 3, pp. 867-875, 2008.

[66] K.-S. Zoannou, D. J. Sapsford and A. J. Griffiths, "Thermal degradation of monoethanolamine and its effect on CO2 capture capacity," *International Journal of Greenhouse Gas Control,* vol. 17, pp. 423-430, 2013.

[67] P. Moser, G. Wiechers, S. Schmidt, J. G. M.-S. Monteiro, C. Charalambous, S. Garcia and E. S. Fernandez, "Results of the 18-month test with MEA at the post-combustion capture pilot plant at Niederaussem – new impetus to solvent management, emissions and dynamic behaviour," *International Journal of Greenhouse Gas Control,* vol. 95, p. 102945, 2020.

[68] A. S. Witkowski and M. Majkut, "The impact of CO2 compression systems on the compressor power required for a pulverized coal-fired power plant in post-combustion carbon dioxide sequestration," *The Journal of Committee on Machine Building of Polish Academy of Sciences,* vol. 59, no. 3, pp. 343-360, 2012.

[69] S. B. Martynov, N. K. Daud, H. Mahgerefteh, S. Brown and R. T. J. Porter, "Impact of stream impurities on compressor power requirements for CO2 pipeline transportation," *International Journal of Greenhouse Gas Control,* vol. 54, pp. 652-661, 2016.